JGR Earth Surface

RESEARCH ARTICLE
10.1029/2023JF007076

Symmetry in Hillslope Steepness and Saprolite Thickness Between Hillslopes With Opposing Aspects

A. M. Donaldson[1], M. Zimmer[1], M.-H. Huang[2], K. N. Johnson[1,3], B. Hudson-Rasmussen[2], N. Finnegan[1], N. Barling[1], and R. P. Callahan[1]

[1]Department of Earth and Planetary Sciences, University of California, Santa Cruz, CA, USA, [2]Department of Geology, University of Maryland, College Park, MD, USA, [3]Department of Integrative Biology, University of California, Berkeley, CA, USA

Key Points:

- Aspect-dependent microclimatic and vegetative differences do not correspond to physical structure between hillslopes
- Similar physical structure between hillslopes may be driven by various aspect-dependent processes leading to similar material loss and production
- A more comprehensive understanding of critical zone development requires integration of past and present biotic and climatic processes

Supporting Information:

Supporting Information may be found in the online version of this article.

Correspondence to:

A. M. Donaldson and M. Zimmer,
amdonald@ucsc.edu;
margaret.zimmer@ucsc.edu

Citation:

Donaldson, A. M., Zimmer, M., Huang, M.-H., Johnson, K. N., Hudson-Rasmussen, B., Finnegan, N., et al. (2023). Symmetry in hillslope steepness and saprolite thickness between hillslopes with opposing aspects. *Journal of Geophysical Research: Earth Surface*, *128*, e2023JF007076. https://doi.org/10.1029/2023JF007076

Received 19 JAN 2023
Accepted 24 MAY 2023

Author Contributions:

Conceptualization: A. M. Donaldson, M. Zimmer, M.-H. Huang, K. N. Johnson, N. Finnegan
Data curation: A. M. Donaldson, M.-H. Huang, K. N. Johnson, B. Hudson-Rasmussen, N. Barling
Formal analysis: A. M. Donaldson, M.-H. Huang, K. N. Johnson, R. P. Callahan
Funding acquisition: A. M. Donaldson, M. Zimmer, K. N. Johnson

Abstract The structure of the critical zone (CZ) is a product of feedbacks among hydrologic, climatic, biotic, and chemical processes. Past research within snow-dominated systems has shown that aspect-dependent solar radiation inputs can produce striking differences in vegetation composition, topography, and soil depth between opposing hillslopes. However, far fewer studies have evaluated the role of microclimates on CZ development within rain-dominated systems, especially below the soil and into weathered bedrock. To address this need, we characterized the CZ of a north-facing and south-facing slope within a first-order headwater catchment located in central coast California. We combined terrain analysis of vegetation distribution and topography with soil pit characterization, geophysical surveys and hydrologic measurements between slope-aspects. We documented denser vegetation and higher shallow soil moisture on north facing slopes, which matched previously documented observations in snow-dominated sites. However, average topographic gradients were 24° and saprolite thickness was approximately 6 m across both hillslopes, which did not match common observations from the literature that showed widespread asymmetry in snow-dominated systems. These results suggest that dominant processes for CZ evolution are not necessarily transferable across regions. Thus, there is a continued need to expand CZ research, especially in rain-dominated and water-limited systems. Here, we present two non-exclusive mechanistic hypotheses that may explain these unexpected similarities in slope and saprolite thickness between hillslopes with opposing aspects.

Plain Language Summary Small differences in solar radiation and water availability between hillslopes facing opposite directions may lead to distinct vegetation and hillslope structures. However, more research is needed to understand the controls and extent of structural differences in the subsurface, especially in rain-dominated landscapes. To investigate the physical and ecohydrologic characteristics between hillslopes that face opposite directions, we combined terrain analysis, soil pit characterization, geophysical surveys and hydrologic measurements taken from two hillslopes facing opposite directions. We found that the hillslope that faced north had higher oak tree density, and higher soil moisture than the hillslope that faced south. These observations match other published studies from a range of landscapes and climates in the northern hemisphere. However, contrary to expectations based on other studies, we found that the surface slope and weathered bedrock thickness were similar between the two hillslopes. Similarities in soil water at 50 cm and increased perched groundwater response on the hillslope that faces south suggest that how water moves within the hillslope and what water is available to plants may alter how rock breaks down. In addition, historic climate and water availability may be important to understand the present-day hillslope structure.

1. Introduction

The diversity of landforms on Earth's surface is intrinsically linked to the spatial distribution of the major components of climate: precipitation and air temperature (Perron, 2017; Sharp, 1982). Studies of the development of the critical zone (CZ), which extends from the top of vegetation to fresh bedrock, investigate the feedbacks among climatic conditions, hydrologic and ecological processes, underlying geology and tectonic stresses at time scales from individual precipitation events (Sólyom & Tucker, 2004) to millions of years (Lebedeva & Brantley, 2020). Differences in subsurface CZ structure (e.g., permeability, porosity, thickness) have been attributed to climate (Anderson et al., 2013, 2019), underlying lithology (Buss et al., 2017; Callahan et al., 2022; Hahm et al., 2019), subsurface water movement (Lebedeva & Brantley, 2013, 2018; Rempe & Dietrich, 2014) and regional tectonics (Ma et al., 2021; Moon et al., 2017; Riebe et al., 2001; St. Clair et al., 2015). However, the ability to identify

Investigation: A. M. Donaldson, M.-H. Huang, B. Hudson-Rasmussen, N. Barling
Methodology: A. M. Donaldson, M. Zimmer, M.-H. Huang, K. N. Johnson, B. Hudson-Rasmussen
Project Administration: A. M. Donaldson, M. Zimmer
Resources: A. M. Donaldson
Software: M.-H. Huang, B. Hudson-Rasmussen
Supervision: M. Zimmer
Validation: A. M. Donaldson
Visualization: A. M. Donaldson, M.-H. Huang, K. N. Johnson
Writing – original draft: A. M. Donaldson, M. Zimmer
Writing – review & editing: A. M. Donaldson, M. Zimmer, M.-H. Huang, K. N. Johnson, B. Hudson-Rasmussen, N. Finnegan, N. Barling, R. P. Callahan

the above and belowground causal mechanisms on CZ development and function across diverse landscapes is currently lacking. A better understanding of the relationship between climate and CZ development is essential to disentangle dominant drivers, improve process-based Earth Systems models (Fan, Clark, et al., 2019; Fan, Grant, & Anderson, 2019, predict environmental responses to climate change (Ferdowsi et al., 2021; Maxwell & Shobe, 2022), and manage water resources (Fan, Clark, et al., 2019; Fan, Grant, & Anderson, 2019).

Hillslopes with opposing aspects, or facing opposite directions, provide natural experiments to investigate how small-scale climatic differences control CZ development (Anderson et al., 2014; Chorover et al., 2011). For example, in the northern hemisphere, higher solar radiation inputs on south-facing slopes (SFS) generate hotter and drier conditions compared to north-facing slopes (NFS), which receive less solar radiation per unit area (Pelletier et al., 2017; Poulos et al., 2012; Yetemen et al., 2015). NFS remains cooler and wetter, which promotes the establishment of mesic species and denser vegetation structure (Armesto & Martinez, 1978; Desta et al., 2004; Zapata-Rios et al., 2016). These aspect-dependent differences in vegetation have been shown to be key factors contributing to physical CZ asymmetries in water-limited ecosystems (Pelletier et al., 2017; Smith & Bookhagen, 2020).

Researchers have used these small spatial scale differences in solar radiation and vegetation to develop a set of common expectations of aspect-dependent hillslope-scale CZ characteristics (Pelletier et al., 2017; Regmi et al., 2019). Specifically, a common expectation is that lower vegetation densities on SFS will reduce soil surface infiltration capacity, enhancing surface runoff and the promotion of sediment transport (Gutierrez-Jurado et al., 2006; Yetemen et al., 2015). The result of these feedbacks may be the development of less steep SFS slopes compared to densely vegetated NFS with lower sediment transport efficiency (Inbar et al., 2018; Istanbulluoglu et al., 2008). That said, this is not universally true; case studies have shown that colluvial sediment transport processes (e.g., animal burrowing and floral-bioturbation) may dominate soil-mantled hillslopes (McGuire et al., 2014; Roering et al., 2002). In these places, hillslope asymmetry may deviate from our current expectations (Pelletier et al., 2017). For example, colluvial sediment transport can increase with vegetation density (Hughes et al., 2009; McGuire et al., 2014), which may enhance erosion on NFS and make them less steep than SFS. Therefore, despite the expectation that SFS will be less steep than NFS, competition exists between sediment transport processes across landscapes, making universal expectations challenging to identify.

Another common expectation is that aspect-dependent differences in vegetation density contribute to differences in hydrologic flowpaths, and thus, the degree of subsurface chemical weathering (Chorover et al., 2011). Specifically, more vegetation on NFS can increase organic matter and contribute to finer soil texture, which increases soil water retention capacity and promotes soil development (Anderson et al., 2014; Gutierrez-Jurado et al., 2006). Below the soil, higher soil water content may allow for deeper recharge into the saprolite, which contributes to thicker, more weathered saprolite on NFS (Garcia-Gamero et al., 2021; Langston et al., 2015). However, these expectations are largely based on snow-dominated catchments where other processes, such as freeze-thaw cycles and snowmelt, can compound the role of vegetation across aspect (Anderson et al., 2013; Befus et al., 2011; Nielson et al., 2021; West et al., 2019). Therefore, despite the expectation that NFS will have a deeper subsurface CZ, this common expectation must be tested in rain-dominated catchments to confirm its transferability across landscapes.

Recent aspect-based studies in rain-dominated catchments have suggested that the role of microclimates on CZ structure is more complex than previously documented in snow-dominated studies (Inbar et al., 2018; Kumari et al., 2020). Hudson-Rasmussen et al. (2023) combined seismic refraction geophysical surveys with geochemistry data from Pedrazas et al. (2021) to investigate subsurface weathering between opposing slopes within a rain-dominated oak woodland underlain by sedimentary rocks. While they observed slope-aspect differences in vegetation, hillslope steepness, and soil depth, there were no clear aspect-dependent differences in saprolite thicknesses. They suggested that the observed symmetry in saprolite thickness is a relic of past wetter climatic conditions and additional time is required to produce saprolite asymmetry.

Here, we test the current expectation that NFS are wetter, steeper, and have thicker soil and saprolite compared to SFS within a rain-dominated catchment underlain by sedimentary rocks. To do so, we identified a sedimentary catchment with end-member vegetation assemblages (i.e., grasses vs. trees) in the central California Coast Range and coupled topographic, hydrologic, pedologic, and geophysical data from two adjacent hillslopes with opposing aspects. Based on our observations, we introduce testable hypotheses that represent exciting frontiers within the ecohydrologic and CZ science communities.

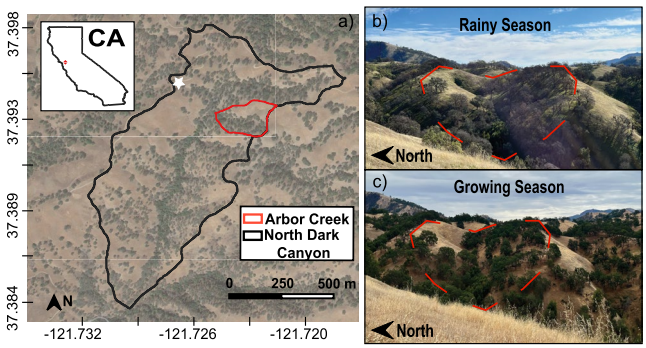

Figure 1. (a) Arbor Creek Experimental Catchment area delineated (red) within the larger North Dark Canyon Watershed (NDC, black) and inset map of California, (b) Arbor Creek Experimental Catchment during the rainy season (February 2022) and (c) Arbor Creek Experimental Catchment during the growing season (June 2022). White star in panel (a) indicates where the rainy season and growing season photos of Arbor Creek Experimental Catchment were taken.

2. Site Description

The study site is a small (0.04 km^2) headwater catchment with an ephemeral stream that drains to the west, referred to as "Arbor Creek" (37.393, −121.723) within the North Dark Canyon Watershed (0.77 km^2). Arbor Creek Experimental Catchment is located within the University of California Blue Oak Ranch Reserve (BORR; Figure 1) from 720 to 790 m above sea level. This reserve is located within the Mt. Diablo Range, ~24 km northeast of San Jose, California, USA.

2.1. Geologic and Tectonic Setting

The overall geologic setting of the study site is a recently uplifted coastal range with relatively low relief uplands (600–800 m above sea level) that are dissected by deep canyons (up to ~500 m) where large landslides are common (Page, 1999). The study site has no recorded Pleistocene glaciation or peri-glaciation (Marshall et al., 2021). The underlying geology of the study site has been mapped differently depending on the scale and purpose of investigation from local lithotectonic units observable in an outcrop (Raymond, 2014) to regional tectonic, deformation, and accretion studies that prefer to use the Berkland et al. (1972) belt terminology (Bolhar & Ring, 2001; Ernst, 2011; Raymond, 2018). At the highest resolution of geologic mapping of 1:24,000, Dibblee and Minch (2005) characterized the area as Franciscan Assemblage comprised of massive to bedded metagraywacke sandstone, moderately to pervasively sheared shale and melange units (Crawford, 1975), bedded chert, greenstone, and blueschist. In its most general form, the surrounding region has been mapped broadly as "Franciscan complex undifferentiated," Great Valley Sequence, and the controversial extension of the Eastern Belt/Yolla Bolly Unit with major rock types described as semi-schistose metawacke, meta-mudrock, metachert, and metabasite (Raymond, 2018; Wentworth et al., 1999). Our observations from outcrops within the study site suggest that locally, the dominant rock types are sequences of metagraywacke sandstone, shale, slatey shale with no evidence of chert, blueschist, or melanges, which is best described by the characteristics of the Yolla Bolly Unit and the Great Valley Sequence.

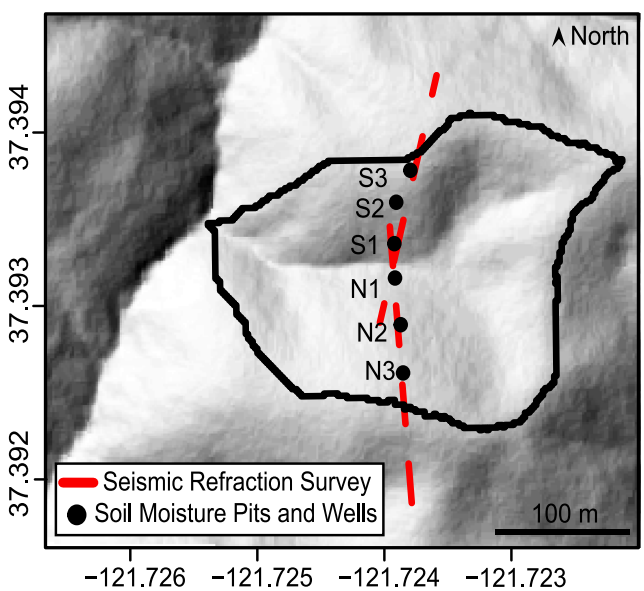

Figure 2. Hillshade of Arbor Creek Experimental Catchment showing instrumentation stations with the location of soil moisture sensors, groundwater wells (black circles; S3, S2, S1, N1, N2, N3) and seismic refraction transects (red dashed lines).

2.2. Climate and Vegetation

Blue Oak Ranch Reserve has a Mediterranean climate characterized by cool, wet winters and warm, dry summers. The average annual rainfall is 600 mm (standard deviation (SD) = 200 mm) from 2012 to 2021 and average air temperature of 8°C in January and 25°C in August (http://www.wrcc.dri.edu/weather/ucbo.html). Nearly all precipitation falls as rain between November and April, and the oak tree growing season extends from April to November.

This study area is characterized as a mixed oak savanna-woodland, where vegetation composition throughout the reserve is generally aspect-dependent (Figure 1). Within Arbor Creek Experimental Catchment, the NFS is a deciduous oak woodland dominated by blue oak (*Quercus douglasii*) and California black oak (*Quercus kelloggii*), with California bay laurel (*Umbellularia californica*) and California buckeye (*Aesculus californica*) present in the lower riparian area. The SFS is predominantly a perennial grassland (i.e., *Bromus diandrus* and *Elymus glaucus*) with sparse blue oak present at lower portions in the catchment that have a southeast slope angle.

3. Methods

The principal study transect within Arbor Creek Experimental Catchment covers two hillslopes, one NFS and one SFS, that drain to the ephemeral stream channel. On the transect, we established six instrumented stations across different landscape positions: near-stream, mid-slope, and near-ridge (Figure 2).

3.1. Terrain Analysis

We explored relationships between insolation, hillslope gradient, and vegetation using 1-m resolution 2020 LiDAR data collected for Santa Clara County (U.S. Geological Survey, 2020). We downloaded a bare-earth raster model of these data produced by the U.S. Geological Survey, and a raster of unfiltered first-return (vegetation top) data, both from opentopography.org. The first-return data were reprojected and resampled to align with the bare-earth data. Vegetation height was calculated by subtracting the bare-earth data from the first-return (vegetation top) data. A binary tree/no tree layer was generated with a 2-m vegetation height threshold after experimenting and spot checking this threshold against field knowledge. Chaparral is not very common in these areas, but where present is included in the "no tree" category. Insolation was modeled for the bare-earth data in ArcGIS Desktop using the Area Solar Radiation tool as direct radiation, diffuse radiation, and duration of radiation for the solstices, equinox, and annual totals. In addition, slope, aspect, and degrees from south were calculated from the bare-earth data. We compared the distributions of these terrain features in Arbor Creek Experimental Catchment to other watersheds in the same local region of the Diablo Range with similar lithology and geomorphic context to assess if the terrain features observed at our study site were representative of the larger region. We excluded infilled and fault-influenced valleys along the San Andreas Fault and excluded areas to the north within the Arroyo Hondo watershed that have much faster incision rates and hence steeper terrain.

3.2. Precipitation Measurements, Soil Characterization and Moisture

At the ridge of the NFS, we installed a weather station (ClimaVUE50, Campbell Scientific; Logan, Utah) to record precipitation inputs at 10-min intervals from 1 October 2020 to 30 September 2021 (2021 water year). We excavated soil to refusal (∼1 m) and characterized the soil and top of saprolite at the near-stream, mid-slope, and near-ridge positions. We delineated soil horizons, depth to saprolite, and characterized parent material within the vertical pit faces. We define the soil as the organic or unconsolidated material that extends from the ground surface to the top of the "C" horizon. The measurement accuracy of the EC-5 sensors is 0.025 m^3/m^3 and 0.045 m^3/m^3 for sandy loam and silty loam soil, respectively (Kanso et al., 2020). We recorded soil VWC (cm^3/cm^3) at 10-min intervals from 1 October 2020 to 30 September 2021 (2021 water year).

We compared soil moisture across landscape positions within storm events, between storm events, and over the dry summer period. Storm events were defined with an event separation method that relied on two thresholds: minimum precipitation amount and minimum period without precipitation inputs (Wiekenkamp et al., 2016). A minimum precipitation amount of 1 mm was chosen because it was within the scope of precipitation sensor error and reduced the likelihood of analyzing precipitation inputs caused by fog that would not produce soil moisture response. A minimum period without precipitation of 12 hr was chosen because durations less than 12 hr did not fully capture soil moisture responses to incoming precipitation and durations of 24 hr led to lengthy events (>20 days) that were not representative of observed on-site storm lengths. We began the analyses on 21 January 2021 once all the soil moisture probes were operational, and a total of 13 precipitation events were delineated. The beginning of the summer period began on 25 April 2021, which was the date of the last precipitation input for that water year.

3.3. Saprolite Lithology and Perched Groundwater Measurements

We characterized the dominant saprolite lithology and the presence of a shallow, perched, and transient groundwater response at the saprolite-weathered bedrock interface by drilling boreholes and installing wells. Notably, the deeper, persistent water table is below the depth of observations that are pertinent to this work. Adjacent to soil pits, we hand-augered 2-inch boreholes to refusal (∼1 m) and then drilled with a gas-powered backpack drill (Shaw Tool Ltd., Yamhill, Oregon) to 3–5 m, constrained by the drill's ability to advance through the material. On the NFS, the well depths were 3.33, 3.96, 3.80 m at the near-stream, mid-slope, and near-ridge landscape positions, respectively. On the SFS, the well depths were 3.10, 4.20, 4.67 m at the near-stream, mid-slope, and near-ridge, respectively. We characterized exhumed borehole samples by lithology type (i.e., shale vs. sandstone; Table S2 in Supporting Information S1).

Within each borehole, we installed wells to measure perched groundwater levels every 10-min using pressure transducers (±0.1 mm resolution; Solinst, California). We screened the wells from the bottom of the adjacent soil pit (∼1 m) to the bottom of the borehole to isolate hydrologic responses between the soil and underlying saprolite.

Table 1
Geometric Information for the Seven Seismic Refraction Surveys

Line #	Line name	Date collected	Geophone spacing (m)	Shot spacing (m)	Stack #	Seismic line length (m)
1	SFS_deep	10 August 2021	3	8	8	144
2	SFS_shallow1	10 August 2021	1	1	2	48
3	SFS_shallow2	10 August 2021	1	1	2	48
4	NFS_deep	11 August 2021	4	8	8	192
5	NFS_shallow1	11 August 2021	1	1	2	48
6	NFS_shallow2	11 August 2021	1	1	2	48
7	NFS_shallow3	11 August 2021	1	1	2	48

Due to the long screen intervals, it should be noted that we cannot definitely state which depth perched groundwater response originates. However, we believe that the depth to the refusal of the drill represents a transition from more friable to less friable material (thus a strong contrast in permeability) that may contribute to transient saturated conditions. We quantified the duration of perched groundwater response for each well as the percent of time that perched groundwater was present (i.e., sensor readings were ≥0.1 m) from 27 January 2021 to 25 April 2021. This date range presents the period from when all water level sensors were installed to the date of the last precipitation input for that water year.

3.4. Seismic Refraction

In August 2021, we conducted an active source seismic refraction campaign to investigate subsurface weathering patterns within the CZ. We completed seven surveys along the study transect, with four on the NFS and three on the SFS. We used two 24-channel Geode seismographs (Geometrics; San Jose, California). We generated the seismic source by swinging a sledgehammer onto an aluminum plate with 2–8 stacked shots adjacent to the survey lines. For the surveys, we used geophone spacing that ranged from 1 to 4 m and shot intervals that ranged from 1 to 8 m (Table 1). It should be noted that the seismic refraction surveys cannot be used to determine soil depth because the source frequency of hammer shots (~30 Hz) was not high enough to sufficiently resolve the seismic velocity of material less than 1 m depth range. We determined the topographic geometry for the seismic model from a 1.5 m spatial resolution Digital Elevation Model collected from an airborne LiDAR mission in 2006.

For each survey, we used the software *Pickwin* (Geometric Inc.) to pick the first P-wave (primary wave from the active seismic source) arrival time to each geophone location. Prior to the inversion, the travel-time data from the NFS and SFS were combined to create a single set of inputs for the inversion on each hillslope. We then performed a Transdimensional, Hierarchical, Bayesian inversion approach with reverse-jump Markov Chain Monte Carlo (THB rjMCMC) from Huang et al. (2021). The initial velocity model was proposed by interpolation of 40 model cells that are randomly distributed in the model domain, and the velocity was ranged from 300 m/s at the surface to 5,000 m/s at the bottom of the model. We randomly iterated the velocity model to create, delete, or move a model cell. We also allowed a random model cell to vary its velocity within the range of 300 and 5,000 m/s. As the measurement uncertainty is not known, it is inferred by the noise hyperparameter. The THB rjMCMC method randomly accepts or rejects the proposed model based on the algorithm proposed by Metropolis et al. (1953). This method calculates a mean model distribution from an ensemble of posterior velocity models after burn-in that can fit the measured P-wave travel time equally well. With this approach, we can reliably estimate measurement uncertainty as well as model resolving power at depth. After $\sim 6 \times 10^5$ iterations of this inversion approach, we used the estimated mean velocity of the ensemble posterior distribution to create a two-dimensional cross section of the best-fit subsurface seismic velocity structure. The interpreted transitional depths in subsurface structure are an approximation due to model structure and limitations (i.e., ray path coverage, smoothing factors, and cell size), but combined with ground-truthed observations of boreholes excavated materials provide a useful approach to identify seismically significant shifts in CZ structure. For more details on post-processing of the seismic velocity model, refer to Huang et al. (2021).

From our resulting velocity models described above, we calculated the vertical velocity gradient, defined as the change of P-wave seismic velocity with depth. Maxima in vertical velocity gradients have been shown to correlate with a transition from highly disaggregated or weathered material to more pristine, low porosity bedrock (Flinchum et al., 2022). Thus, we used vertical velocity gradient profiles across our study transect to identify potential transitions in CZ structure (i.e., porosity, lithology). We calculated the thickness of the saprolite along the survey transect by subtracting the land surface elevations from the average depth of the highest vertical velocity gradient and the corresponding seismic velocity contour, which has previously been shown to represent a transition to saprolite (Flinchum et al., 2018; Hudson-Rasmussen et al., 2023). We then binned the data into 5 m intervals (horizontal resolution of seismic data) and compared the difference in the calculated saprolite thickness between the max velocity gradient method and corresponding contour method between hillslope aspect. We used the Shapiro-Wilk Normality Test to test for normality across the different data sets, which determines whether data are normally (parametric) or not normally (non-parametric) distributed (Yazici & Yolacan, 2007). We determined whether the differences between slope-aspects across landscape positions are statistically significant using *t*-tests for parametric data and the Mann-Whitney U tests for non-parametric data (McKnight & Najab, 2010).

4. Results

4.1. Terrain Characteristics

Insolation has the greatest influence on tree presence in our study area. Above about 2,500 WH/m^2, we see a decrease in the ratio of hillslope pixels classified as trees (Figure S1 in Supporting Information S1, dashed line). This pattern can be observed qualitatively on the landscape most readily when looking at the vegetation contrast between adjacent NFS and SFS, which average around 1,500 WH/m^2 (~60% tree pixels) and 3,500 WH/m^2 (~20% tree pixels), respectively, in this local region (e.g., Figure 2; Figure S2 in Supporting Information S1). Within Arbor Creek Catchment, hillslope pixels oriented within 45° of North and South have similar distributions of slope angles (mean slope of 23.7° on NFS and 24.4° on SFS) (Figure 3a). Despite variability in hillslope orientation due to stream network shape, when comparing pixels across the larger region, NFS and SFS also have similar slope angles (mean slope of 24.7° on NFS and 23.2° on SFS).

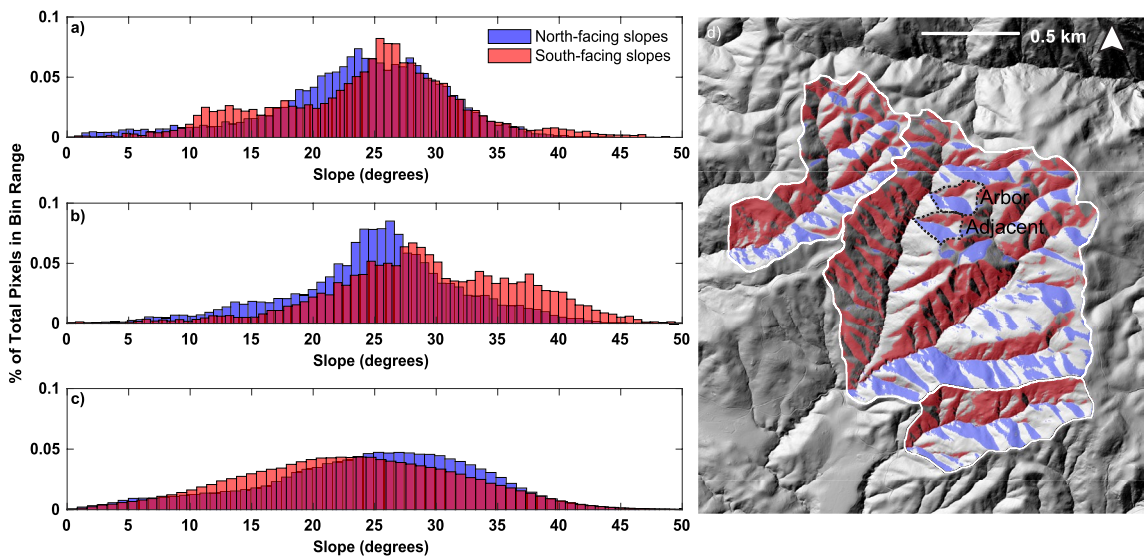

Figure 3. Slope distributions (a) for Arbor Creek Experimental Catchment (delineated in black (d)), for an (b) adjacent catchment to the south with similar solar orientation (delineated in black (d)), and for a (c) broader sample of catchments in the local region with similar geomorphology and lithology (delineated in white (d)). NFS's are shaded with blue and SFS's are shaded with red.

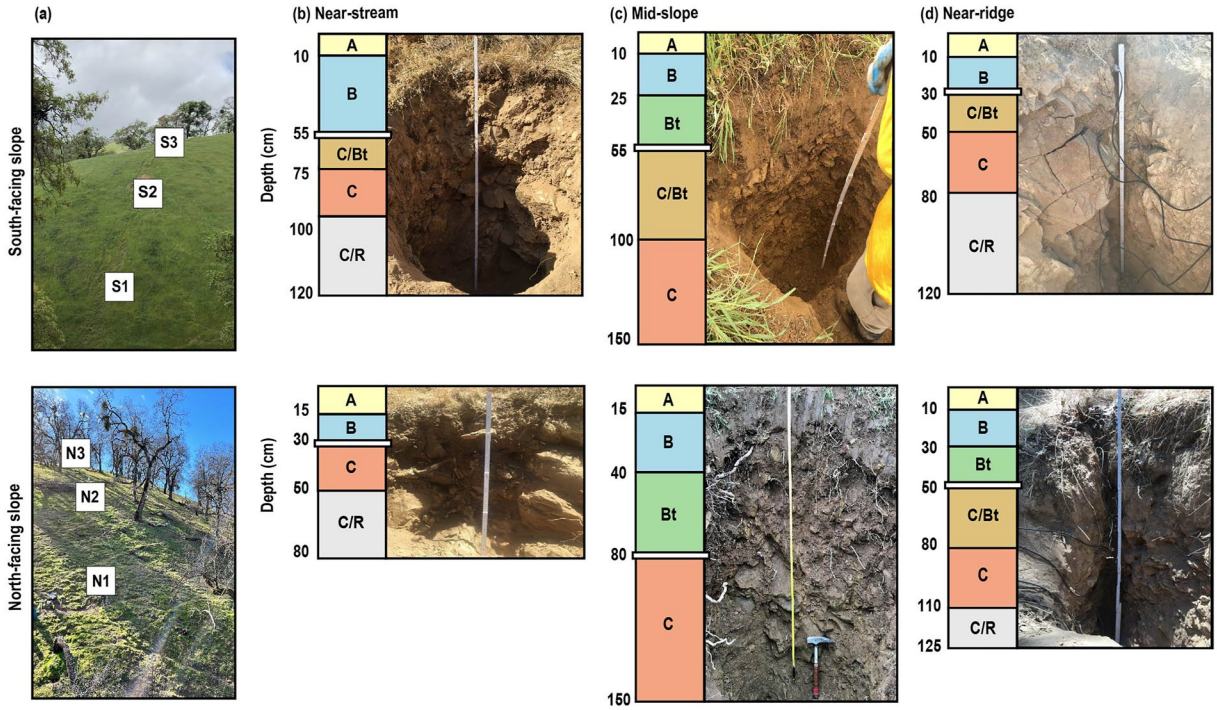

Figure 4. (a) Images of Arbor Creek Experimental Catchment's south-facing slopes and north-facing slopes. Soil pit images with soil horizons delineated at the (b) near-stream, (c) mid-slope and (d) near-ridge landscape positions. White line on the illustrated monolith represents the transition between soil to saprolite.

4.2. Soil Characteristics

Across the six soil pits, the soil depth ranged from 30 to 80 cm, with a mean depth of 51 cm (Table S1 in Supporting Information S1). On the NFS, soil depth varied by landscape position, with the shallowest soil depth occurring at the near-stream position (30 cm), the deepest soil depth at the mid-slope (80 cm) and intermediate depth (50 cm) at the near-ridge position. On the SFS, the soil depth was more uniform relative to the NFS; the near-stream and mid-slope both had 55 cm soil depths, while the near-ridge soil depth was only 30 cm (Figure 4).

4.3. Saprolite Characteristics

The seismic refraction mean velocity, vertical velocity gradient, and coefficient of variation are shown in Figure 5, showcasing the similarity in saprolite thickness between slope-aspects. The max vertical velocity gradient best corresponds to the depth at which the seismic velocity ranges from 1,200 to 1,400 m/s (Figure S3 in Supporting Information S1). This range is similar to velocities used to distinguish the saprolite-weathered bedrock transition in sandstones and mudstones (1,300 m/s; Hudson-Rasmussen et al., 2023) and granitic gneiss (1,400 m/s; Flinchum et al., 2019). We therefore inferred that the transition between the saprolite and weathered bedrock occurred within the range of the max velocity gradient, the depth to the 1,200 and 1,400 m/s seismic velocity contour. We observed the thickness of the saprolite to generally decrease from the ridge to the stream channel (Figure 6). These geophysical observations indicate that the saprolite thickness is similar between hillslopes with opposing aspects (Figure 6). Though the maximum vertical velocity gradient is systematically higher on the NFS (686 m/s/m) compared to the SFS (277 m/s/m). Based on the depth to the maximum gradient, the average saprolite depth was 6.6 $\pm$ 0.31 m and 5.7 $\pm$ 0.32 m on the NFS and SFS, respectively, and not statistically significant between slope-aspects ($t = 1.89$, p-value = 0.07). Based on the depth to the 1,200 m/s contour, the average saprolite depth was 6.1 $\pm$ 0.42 m and 5.6 $\pm$ 0.27 m for the NFS and SFS, respectively, which were not statistically different ($t = 0.95$, p-value = 0.34). Finally, using the 1,400 m/s velocity contour, the saprolite depth, 7.5 $\pm$ 0.64 m and 7.3 $\pm$ 0.49 m for the NFS and SFS, respectively, was also not statistically different ($W = 145.5$, p-value = 0.72). The root-mean-square error misfit evolution, mean misfit, a SD of the misfit in the mean velocity model, modeled travel time and observed travel time and raypath density of the mean velocity model are provided in Supporting Information S1 for the NFS and SFS (Figures S4 and S5 in Supporting Information S1, respectively).

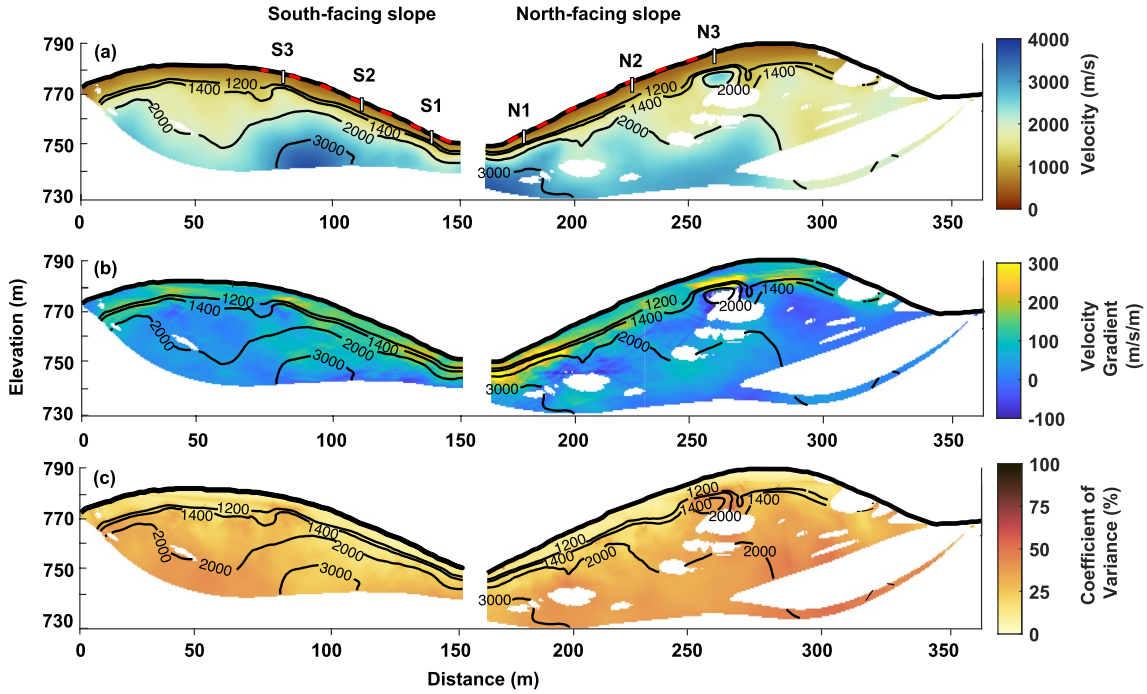

Figure 5. (a) Mean seismic refraction velocity model, (b) mean vertical velocity gradient, and (c) coefficient of variation for velocity model (inferred as model uncertainty) with 1,200, 1,400, 2,000, and 3,000 m/s velocity contours. Dashed red lines in panel (a) represent the hillslope length further analyzed for saprolite thickness. Vertical white bars in panel (a) represent the well locations and extent.

Below the maximum vertical velocity gradient, the seismic velocity increased from ~1,300 to 3,000 m/s on average at 26 m (SD 10 m) and 49 m (SD 11 m) below the ground surface on the SFS and NFS, respectively. The increase in the seismic velocity could be due to a gradually decreasing porosity (Figure 5; Flinchum et al., 2022; Gu et al., 2020). This transition most likely represents the transition from weathered bedrock (more competent than the saprolite above) to more pristine, low porosity material. The P-wave velocity of pristine (not chemically altered) sandstone with <20% porosity has been shown to be >3,800 m/s (Geldart & Sheriff, 2004). However, based solely on the seismic velocity data, we are unable to distinguish between weathered bedrock with low fracture density and fresh bedrock with high fracture density.

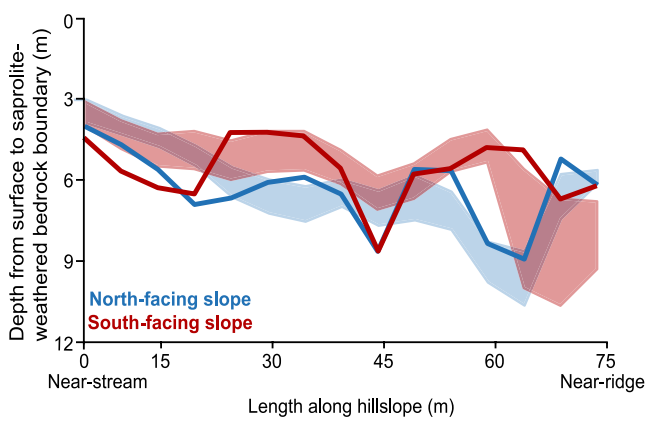

Figure 6. Average saprolite depth based on the depth to the 1,200 m/s velocity contour and 1,400 m/s velocity contour (top and bottom of shaded region, respectively) and the max velocity gradient (bold lines) for the north-facing slopes (blue) and south-facing slopes (red) within Arbor Creek Experimental Catchment.

4.4. Soil Moisture and Perched, Transient Groundwater Responses

During the 13 delineated storm events, the soil VWC was similar between slope-aspects except at the 10 cm mid-slope position (Figure 7). At the near-stream position, the average 10 cm soil VWC was 0.16 and 0.18 on the SFS and NFS, respectively. At the mid-slope position, the 10 cm soil VWC was on average 0.19 and 0.28 on the SFS and NFS, respectively. At the near-ridge position, the 10 cm soil VWC was on average 0.22 and 0.25 on the SFS and NFS, respectively. Deeper within the soil, at the near-stream position, the 50 cm soil VWC was on average 0.16 and 0.18 on the SFS and NFS, respectively. At the mid-slope position, the 50 cm soil VWC was on average 0.25 on both the NFS and the SFS. At the near-ridge position, the 50 cm soil VWC was on average 0.24 and 0.27 on the SFS and NFS, respectively. Notably, at the near-ridge position, the SFS 50 cm soil VWC had flashy responses that increased the soil VWC above the NFS 50 cm soil VWC (Figure 7).

Between storm events, the soil VWC on the SFS was generally drier than the NFS (Figure 7). Specifically, between storm events, the 10 cm soil VWC on the SFS was on average 0.13, 0.17, and 0.22 at the near-stream, mid-slope, and near-ridge positions, respectively. The NFS 10 cm soil VWC was 0.16,

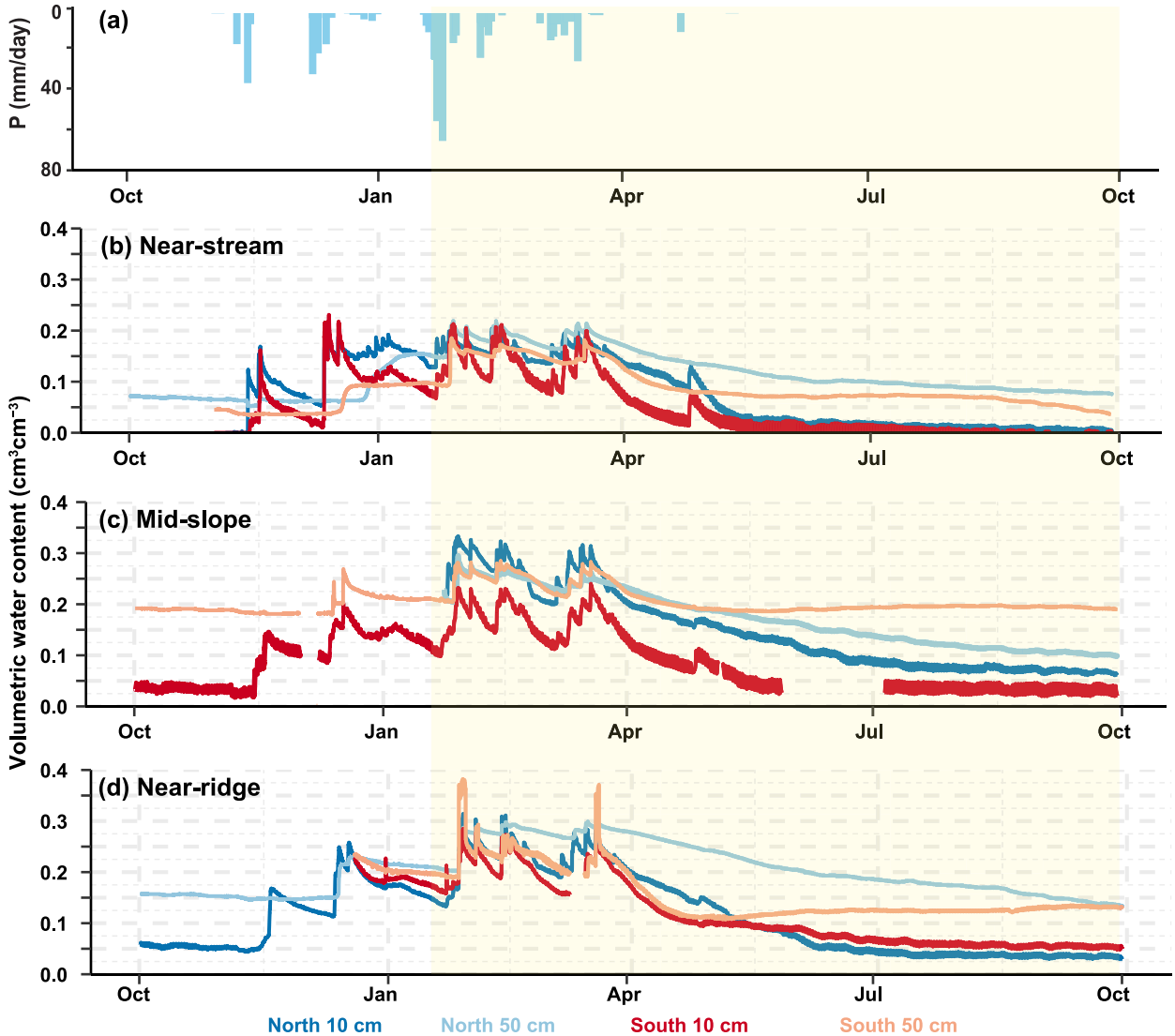

Figure 7. (a) Precipitation time series; Soil moisture at the (b) near-stream, (c) mid-slope, and (d) near-ridge landscape positions. At each landscape position, 10 cm (light) and 50 cm (dark) depths are shown for north-facing slopes (blues) and south-facing slopes (reds). Missing data are due to sensor malfunction. The yellow shaded region indicates the time period when soil moisture was compared in this study (21 January 2021–30 September 2021).

0.26, and 0.22 at the near-stream, mid-slope, and near-ridge positions, respectively (Figure 7). Deeper within the soil, at the near-stream position, the 50 cm soil VWC was on average 0.16 on the SFS and 0.18 on the NFS. At the mid-slope position, the 50 cm soil VWC was 0.24 on both the SFS and NFS. At the near-ridge position, the 50 cm soil VWC was 0.24 on the SFS and 0.27 on the NFS (Figure 7).

At the start of the summer 2021, the soil VWC was higher on the NFS compared to the SFS, except at the 50 cm depth mid-slope position where the soil VWC was similarly 0.19 (Figure 7). From April to May, the SFS dried down more than the NFS across all landscape positions and depths. By July, the 10 cm soil VWC dried down below 0.06 on both the NFS and SFS. At the 50 cm depth, the SFS soil VWC drying had plateaued in June while the NFS continued to dry down until September (Figure 7). At the end of the growing season (October), the soil VWC was similar between slope-aspects across all landscape positions and depths, except at the mid-slope position, 50 cm depth, where the NFS was 0.09 drier than the SFS.

Observed water levels in boreholes indicated higher perched groundwater response on SFS compared to NFS at the mid-slope and near-ridge landscape positions (Figure 8). During the period of observation for transient, perched groundwater (27 January 2021–25 April 2021), water levels responded to incoming precipitation events

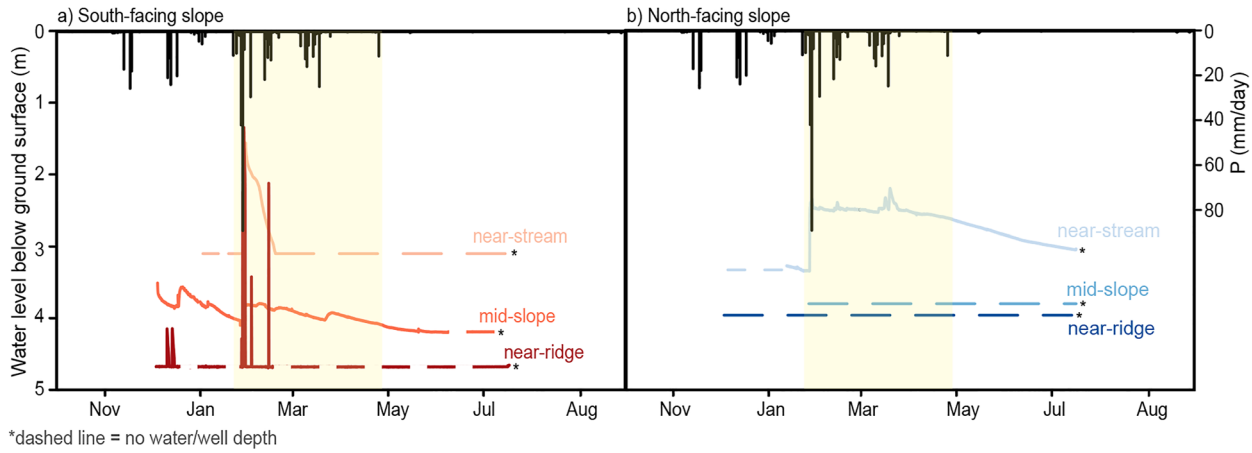

Figure 8. (a) South-facing slopes groundwater time series and (b) north-facing slopes groundwater time series during the 2021 water year for the near-stream, mid-slope and near-ridge landscape positions. Missing data at the beginning of the water year were due to delayed sensor installation and dashed lines represent no water present at the bottom of the well. The yellow shaded region indicates the time period when perched groundwater duration was quantified for this study (27 January 2021–25 April 2021).

across all landscape positions on the SFS, but only responded at the near-stream position on the NFS. Here, the dominant lithology is shale, which differs from the other sandstone-dominated landscape positions. On the NFS, perched groundwater was measurable 99%, 0%, and 0% of the observation period for the near-stream, mid-slope, and near-ridge positions, respectively. On the SFS, perched groundwater was measurable 21%, 98%, and 2% for the near-stream, mid-slope, and near-ridge positions, respectively. While the perched groundwater level at the SFS mid-slope was sustained throughout the observation period, perched groundwater levels at the near-stream and near-ridge positions only responded directly to precipitation events.

5. Discussion: Frameworks to Explain the Unexpected Symmetry in Hillslope Steepness and Saprolite Thickness Between Hillslopes With Opposing Aspects

A key goal of CZ science is to understand the relationship between the observed hillslope form and the past and present dominant geomorphic and hydrologic processes operating within the hillslope (Anderson et al., 2021; West et al., 2019). In the case of Arbor Creek Experimental Catchment, we observed similarities in the physical form (e.g., slope, average soil depth, and saprolite thickness) between hillslope aspects, despite distinct differences in microclimates and vegetation. These observations deviate from current common expectations borne out of extensive work in snow-dominated landscapes that suggest cooler, densely vegetated NFS will have steeper slopes, thicker soil, and thicker saprolite compared to warmer, sparsely vegetated SFS (Pelletier et al., 2017). Here, we contextualize our physical observations based on topographic analysis, soil pits, and geophysical measurements with relevant literature and in situ hydrologic measurements (e.g., soil moisture and perched groundwater) to provide potential explanations for the observed hillslope symmetry between aspects. Lastly, we discuss how the observed physical and ecohydrologic characteristics of Arbor Creek Experimental Catchment compare to current slope-aspect conceptual models. Our work highlights the importance of investigating CZ development between slope-aspects in rain-dominated climates.

We introduce two frameworks with non-exclusive mechanisms that may explain the symmetry in slope, and average soil depth and saprolite thickness between hillslopes with opposing aspects (Figure 9). The first framework explores how contemporary environmental conditions promote processes that can contribute to the similarities in the physical CZ of the NFS and SFS within Arbor Creek Experimental Catchment. The second framework considers how past climate and vegetation distributions could contribute to the present-day hillslopes form. Here, we argue that we must consider both frameworks in tandem to fully understand the development of the CZ we see today.

5.1. Contemporary Framework: Present-Day Similarities in Saprolite Weathering and Sediment Fluxes Between Hillslopes With Opposing Aspects

The Contemporary Framework explores present-day mechanisms that may contribute to the observed similarities in average saprolite thickness, soil thickness and slope between hillslopes with opposing aspects. These observed

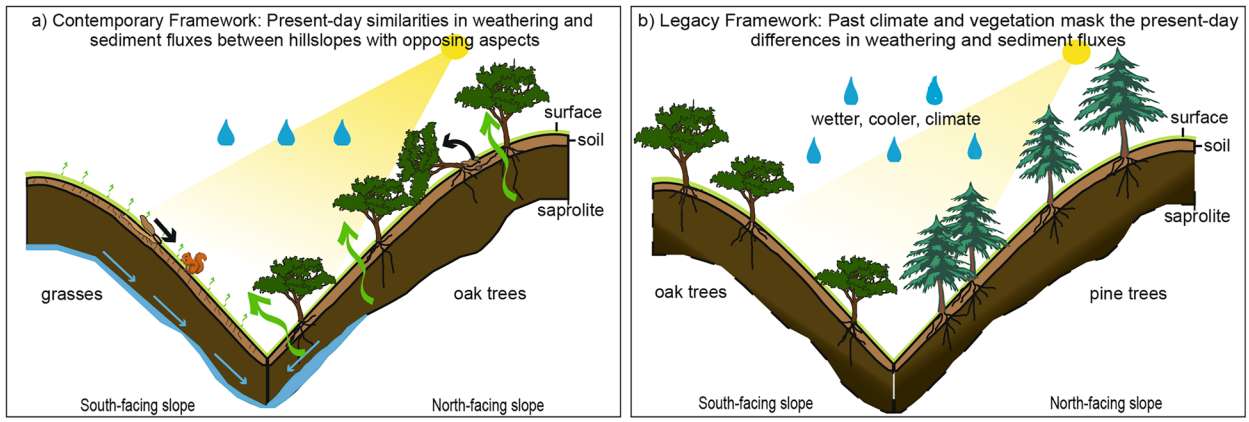

Figure 9. Two frameworks to explain similar hillslope steepness and/or saprolite thickness between hillslopes with opposing aspects. (a) Contemporary Framework: Present-day similarities in saprolite weathering and sediment fluxes between hillslopes with opposing aspects, despite aspect-dependent mechanisms. Similarities in sediment fluxes may be due to a balance between animal burrowing on the south-facing slopes (SFS) and wind-throw on the north-facing slopes (NFS). Similarities in saprolite weathering may be due to a balance between hydrologic dominated weathering on the SFS and hydrologic and biotic weathering on the NFS. (b) Legacy Framework: Past climate and vegetation effects on sediment fluxes and weathering may mask the present-day differences in weathering and sediment fluxes. There may have been similar sediment fluxes and saprolite weathering on the SFS and NFS because of the presence of woody vegetation on both slopes. Alternatively, material loss and production rates may have varied over geologic time, resulting in observed symmetry today. More time may be required under the current vegetative and climatic conditions to produce the expected critical zone asymmetries between aspects due to variable rates over geologic time. The gradient and dashed saprolite-weathered bedrock boundary represent the uncertainty in the past saprolite thickness between hillslope aspects.

similarities suggest that there is a uniform rate of saprolite weathering, soil production, and sediment transport across both slopes. However, we argue that the specific mechanisms driving these similarities vary by aspect.

5.1.1. Saprolite Weathering

One explanation for similar saprolite thickness between hillslopes with opposing aspects is that total saprolite weathering from both chemical and biological processes is uniform between slope-aspects. Within Arbor Creek, we observed more persistent perched shallow groundwater at the saprolite-weathered bedrock interface on the SFS, except at the NFS near-stream position, which is dominated by a different lithology than the rest of the study site (shale instead of sandstone; Figure 8). We hypothesize this perched groundwater presence enhances lateral flow, which accelerates chemical weathering on the SFS (Rempe & Dietrich, 2014; Wang et al., 2021). In contrast, lateral flow toward the stream on NFS may be lower due to limited saturated conditions in the saprolite from oak tree water uptake during the growing season. At the same time, deeply rooted oak trees on NFS may enhance biologically-driven weathering. Therefore, we hypothesize that the cumulative effects of reduced chemical weathering by limited lateral flow and enhanced biological weathering from vegetation on the NFS balance the heightened chemical weathering on SFS and may explain the observed symmetry in saprolite thickness across slopes.

Lateral flow toward the stream channel can occur at a portion of the subsurface where there is a sharp decrease in permeability with depth (Brantley et al., 2017). This perched, lateral drainage of fluids and subsequent replenishment with meteoric fluids is a process that has been proposed to dictate the extent of subsurface chemical weathering (Rempe & Dietrich, 2014). Since our geophysical results show uniform saprolite thickness across slopes, it suggests that if this specific weathering process acted in isolation, it would require lateral flow to be uniform across slopes. However, we observed a more persistent perched groundwater response on the SFS compared to the NFS, suggesting that the SFS may have a higher occurrence of lateral flow.

As stated above, one possible explanation for why we observe symmetry in saprolite thickness between hillslopes with opposing aspects may be due to the deeply rooted oak trees on NFS. Several mechanisms allow plant roots to directly and indirectly promote subsurface weathering processes (Brantley et al., 2017; Pawlik et al., 2016). For example, strain-induced porosity production due to root-wedging between existing fractures may contribute significantly to subsurface weathering (Hayes et al., 2019). Abiotic chemical weathering is strongly influenced by plant water uptake and redistribution, which can alter weathering pathways (Lucas, 2001). As deeply rooted oaks utilize water stored within the saprolite for transpiration (Hahm et al., 2020, 2022), depletion in water content

within the saprolite during the growing season could slow water residence times and increase the production of solutes.

Our observation of similar saprolite thickness across slope-aspects despite differences in vegetation and perched groundwater responses suggest that Arbor Creek Experimental Catchment may serve as an interesting site to investigate the relative importance of saprolite weathering via chemical loss (chemical weathering) and volumetric strain (physical weathering) (sensu Hayes et al., 2019; Riebe et al., 2021). To better understand the controls on subsurface weathering, future research should pair the seismic refraction surveys presented in this study with rock sample bulk geochemistry (e.g., ratios of immobile elements), physical properties analyses (e.g., bulk density, porosity) and a rock physics model (following Hayes et al., 2019). While this approach can not directly discern biotic-induced chemical weathering from water-driven chemical weathering, it can help disentangle the saprolite weathering driven by chemical loss (chemical weathering) and strain-induced porosity production (e.g., root-wedging).

5.1.2. Soil Production and Sediment Transport

Although we did not explicitly investigate erosion or soil production rates within this study, we provide a related hypothesis and justification for a potential driver of symmetry in hillslope steepness and soil thickness between slope-aspects. Based on the observed similarities in average soil thickness and hillslope steepness between aspects, we hypothesize that the soil production and sediment transport are similar despite variations in the dominant erosional and soil production processes operating. Specifically, we hypothesize that the balance between root-induced hillslope stabilization and sediment transport via wind-thrown trees may contribute to a net downslope sediment flux equivalent to the sediment flux on SFS from animal burrowing (Figure S6 in Supporting Information S1).

Small mammal burrowing is potentially a significant mode of sediment transport and soil production in steeply sloped and soil-mantled hillslopes (Black & Montgomery, 1991; Gabet et al., 2003). Although knowledge on the role of animal burrowing on sediment transport is limited to a few species and ecoregions, previous studies have identified a relationship between animal burrows and incoming solar radiation (Hall & Lamont, 2003; Übernickel et al., 2021). For example, Übernickel et al. (2021) conducted an inventory of burrowing animal entrances between NFS and SFS across four study sites with a hydroclimatic gradient in Chile. Their inventory revealed that the majority of small-animal entrances were located on the NFS, which have higher incoming solar radiation in the southern hemisphere (Poulos et al., 2012). They hypothesized that although more food and shelter may be present on the densely vegetated SFS, warmer temperatures on the NFS during the winter months may be favorable habitat for burrowing animals long-term.

Increased woody vegetation on a landscape can also have important implications for sediment transport and soil production due to higher rates of bioturbation (e.g., root decay, and wind-throw) (Gabet & Mudd, 2010). Although little research exists to the authors' knowledge on the causes, effects, and prevalence of wind-throw in oak woodlands, there are several studies investigating the effects of forest regeneration after wind disturbance in mixed-deciduous forests that include oaks (Götmark & Kiffer, 2014; Szwagrzyk et al., 2018). These studies suggest that wind-throw may be an important component of forested disturbance regimes (Cannon et al., 2017), which has unknown consequences for sediment transport and soil production. Therefore, more research is needed to have a better understanding of the potential for wind-throw to promote sediment transport on tree-dominated NFS, compared to grass-dominated SFS.

Similarities in average soil thickness and slope across our study hillslopes suggest that within Arbor Creek Experimental Catchment, prevalent animal burrowing on the warmer SFS may lead to equivalent sediment transport downslope by bioturbation (e.g., animal burrowing and tree-throw) on the NFS over long time scales. Future research to test this would require quantifying animal burrowing between hillslopes with opposing aspects through field surveys (Dixon et al., 2009) and quantifying the sediment flux due to wind-throw by a tree census (Šamonil et al., 2020) or estimating surface roughness with high resolution topographic data (Doane et al., 2021). Additionally, future work using cosmogenic radionuclides to measure hillslope erosion and soil production rates between hillslopes with opposing aspects over long time scales should be used to determine if rates are similar between hillslopes (Anderson et al., 2021; Granger et al., 1996; Heimsath et al., 1999).

5.2. Legacy Framework: Past Climate and Vegetation Mask the Present-Day Differences in Weathering and Sediment Fluxes

One potential mechanism for hillslope steepness and saprolite symmetry between aspects that our study design did not specifically address is the effect of past climates and vegetation distributions on CZ development.

Specifically, despite the expectation that NFS should have steeper slopes and a thicker saprolite compared to SFS, it is possible that the actively eroding landscapes of central coastal California require longer geologic time under the current climatic conditions to produce the expected topographic and subsurface asymmetries (Figure 9b). This is supported by previous studies that have demonstrated that delayed geomorphic adjustments to climatic fluctuations can lead to complex contemporary observations of soil erosion, soil thickness and topographic gradients (Heimsath et al., 1999; Hudson-Rasmussen et al., 2023; Hughes et al., 2009).

The physical structure of the CZ we observe today is an integration of climatic, hydrologic, vegetative, and lithologic processes that occur across a range of timescales. For example, timescales relevant for vegetation shifts can range from decades to centuries (Corlett & Westcott, 2013), while rock weathering patterns emerge over millennia to hundreds of millennia (Lebedeva & Brantley, 2020). For our study, if we estimate a 0.05–0.10 mm/yr erosion rate in the California Central Coast Ranges (sensu Montgomery, 1993), the maximum and minimum time required to develop the observed 6 m thick saprolite is 60,000–100,000 years. Therefore, we can assume that saprolite thickness is not only dictated by the climatic and vegetative conditions during the present-day Holocene but also by the Late Pleistocene (129 to 11.7 Ka). Paleoclimatic records from across California suggest that during the Pleistocene, climatic conditions were cooler and wetter, with potentially more intense precipitation events compared to the present-day Holocene (Daniels et al., 2005; Kulongoski et al., 2009).

Climatic shifts can have important implications for vegetation dynamics (Heusser, 1998) that can influence soil development and erosion, weathering rates and subsurface water storage (Hagedorn et al., 2019; Ivory et al., 2014; Jackson et al., 2000). The transition from the wetter, cooler Pleistocene to the warmer, drier Holocene contributed to a dramatic shift in dominant vegetation composition across California (Heusser, 1998). Pollen analyses from sediment cores and Neotoma (packrat) middens suggest these landscapes were previously dominated by *Pinus* species and that oak woodlands did not become well-established until the early-mid Holocene (Byrne et al., 1991; Cole, 1983; Heusser, 1998; Mensing, 2005). Furthermore, Mensing (2005) suggested that if oak trees were present during the late Pleistocene, it was "likely on the warmer SFS." This suggests that the characteristic grass-dominated SFS and oak-tree dominated NFS we observe today may only be a relatively recent (~10,000 years) phenomenon. Therefore, it is plausible that the legacy of pine and oak trees on the SFS, and the associated rock weathering (Hasenmueller et al., 2017; Pawlik et al., 2016), may contribute to the symmetry in hillslope steepness and saprolite thickness between hillslopes with opposing aspects (Figure 9b).

An approach to investigating this could use numerical modeling to assess how variable climatic conditions (e.g., solar radiation and precipitation) influence vegetation compositions and soil moisture between slope-aspects. For example, Zhou et al. (2013) used an ecohydrological Cellular Automata Tree-Grass-Shrub Simulator to model the role of variable precipitation, solar radiation, and soil moisture on the distribution of juniper pine, grass, and creosote bush shrubs between slope-aspects over 10,000 years. We propose that this type of model could be adapted to investigate the distribution of oaks, pines, and grasses across climatic shifts from the wetter, cooler Pleistocene to the warmer, drier Holocene. Specifically, numerical modeling may be able to predict oak and pine vegetation distributions between slope-aspects and the potential effects on soil water balances. While this does not explicitly relate the vegetation distributions to erosion or subsurface weathering, pairing this vegetation distribution model with a landscape evolution model could begin to tease apart the co-evolution of landscapes with variable vegetation distributions.

5.3. Other Considerations

Spatial variability in hydrologic flow due to preferential flowpaths (e.g., rock fractures and macropores) and lithologic heterogeneity (e.g., rock type and bedrock foliation), which may or may not be aspect-dependent, could be contributing to the subsurface weathering patterns observed (Langston et al., 2015; Leone et al., 2020). For example, within a catchment with aspect-dependent differences in vegetation underlain by sedimentary rocks in Arizona, USA, Leone et al. (2020) combined seismic refraction and electrical resistivity tomography to reveal that saprolite on the SFS was thicker than the NFS. They hypothesized that on the SFS, the well-foliated bedrock dips at an angle that increases hydraulic conductivity, and vertical subsurface hydrologic flow promotes saprolite development. This study highlights that other environmental factors (e.g., lithology) may be a stronger control on hydrologic flowpaths and CZ development than microclimate between hillslopes with opposing aspects. A better understanding of how dominant flowpaths and subsurface structure may influence each other could be garnered with the coupling of more vertically resolved hydrologic measurements, high resolution geophysical

techniques (e.g., ground penetrating radar and electrical resistivity tomography), and tracer or irrigation experiments (Cassiani et al., 2009).

Another consideration that warrants future research is the magnitude of asymmetry that should be expected between hillslopes with opposing aspects in regions across the energy to water limitation gradient (Inbar et al., 2018; Nielson et al., 2021). For example, within a snow-dominated region at the semi-arid Reynold Creek CZ observatory underlain by extrusive igneous rock, Nielson et al. (2021) combined snowpack and soil moisture measurements with seismic refraction surveys to investigate saprolite thickness across an elevational gradient with varying snow accumulation. They observed the greatest saprolite asymmetry at the high elevation site where there was the greatest aspect-dependent difference in snow accumulation. In contrast, the low elevation site had similar snow accumulation between slope-aspects and there were nearly identical saprolite weathering thicknesses. They attributed the lack of weathering asymmetry to similarities in soil VWC and water recharge rates between NFS and SFS. These findings demonstrate that variability in soil VWC and recharge dynamics (e.g., magnitude and extent) can exert a strong control on the variability in soil and saprolite weathering.

Another example of variability in physical CZ asymmetry across precipitation gradients occurred in Southeastern Australia (Inbar et al., 2018). Inbar et al. (2018) observed variability in slope and soil depth differences between slope-aspect along a climogradient with mean annual rainfall from 400 to 2,500 mm. Their results revealed that maximum slope and soil depth asymmetry occurred in the transitional "goldilocks" regime between the wet and dry end member conditions. They hypothesized that variability in CZ physical asymmetry was a result of differences in vegetation cover, fire recurrence intervals, and soil hydraulic properties, which were all highly sensitive to differences in precipitation amounts. Therefore, while we observe strong contrasts in vegetation cover between slope-aspects (grass vs. tree) in Arbor Creek Experimental Catchment, the relatively low precipitation inputs (average 600 mm/yr) relative to the region's high evapotranspiration demand may contribute to the lack of asymmetry observed. This further supports that a one-size-fits all model of aspect controls on hillslope steepness, soil, and saprolite thickness may not capture CZ physical variability across ecoregions important to predict dominant CZ functions.

6. Conclusion

Within a semi-arid, rain-dominated landscape underlain by sedimentary rocks, we used a multidisciplinary approach to investigate the influence of microclimates on CZ structure between hillslopes with opposing aspects. We observed that CZ structure between hillslopes with opposing aspects does not fully align with current conceptual models from the literature that are largely based on snow-dominated landscapes underlain by igneous rocks. We found that on a regional scale, decreased solar radiation correlated with increased tree presence. This aligns with observations within our focus study site, Arbor Creek Experimental Catchment, where the cooler NFS was dominated by oak trees and the warmer SFS was dominated by grasses. However, the hillslope steepness and saprolite thickness was similar between these hillslopes, which was counter to expectations.

We present two frameworks to explain the observed similarity in hillslope steepness, soil and saprolite thickness between hillslopes with opposing aspects. These non-exclusive frameworks highlight the importance of past and present ecohydrologic processes to alter subsurface water storage and movement, which has consequences for long-term CZ development. Further research applying these hypothesized mechanisms across rain-dominated systems with different precipitation magnitudes, vegetation types, and geologic settings can better constrain the prevalence of these potential mechanisms. In addition, the integration of lithologic heterogeneity, paleovegetation distributions and plant-driven alterations in hydrologic flowpaths into numerical models is an exciting frontier in understanding aspect-dependent CZ development. Such research is critically needed to identify the relationship between vegetation, hydrologic flowpaths and weathering, which has important implications for water resource management and ecosystem health in a changing climate.

Data Availability Statement

All data used in the publication are cited in the references and hosted on Consortium of Universities for the Advancement of Hydrologic Science, Inc. (CUAHSI)'s web-based hydrologic information system (Hydroshare). A. M. Donaldson (2023). Symmetry in hillslope steepness and saprolite thickness between hillslopes with opposing aspects, HydroShare, http://www.hydroshare.org/resource/9a9897aa0bb14d20ab4189b98a8439f6.

The THB rj-MCMC software for active source seismic refraction inversion is available in Zenodo (https://doi.org/10.5281/zenodo.4590999; Huang et al., 2021).

Acknowledgments
The authors would like to acknowledge the financial support provided by the Betty and Gordon Moore Foundation under the project title: The California Heartbeat Initiative, National Science Foundation CAREER Grant (Award 2046957), the Instrumentation Discovery Grant through the Consortium of Universities for the Advancement of Hydrologic Sciences, Inc., and the Mildred E. Mathias Graduate Student Research Grant by the University of California Natural Reserve System. The authors would like to acknowledge the financial support granted by the University of California, Santa Cruz through the Kathryn D. Sullivan Impact Award and the Zhen and Wu Memorial Fund Award. The authors thank past and present members of the Zimmer Watershed Hydrology Lab, namely, Chris Causbrook, Peter Willits, Michael Wilshire and Lauren Giggy for support in the lab and field. Members of the California Heartbeat Initiative-Freshwater program, Todd Dawson, Jim Norris, and Collin Bode provided thoughtful guidance and key technical assistance throughout the project. In addition, the authors would like to thank Zac Harlow and Zac Tuthill for land access and troubleshooting enthusiasm. The authors are grateful to Editor Dr. Amy East, Associate Editor Dr. Seulgi Moon, Dr. Brady Flinchum, Dr. Eve-Lyn S. Hinckley, and one anonymous reviewer who provided valuable comments on this manuscript.

References

Anderson, R. S., Anderson, S. P., & Tucker, G. E. (2013). Rock damage and regolith transport by frost: An example of climate modulation of the geomorphology of the critical zone. *Earth Surface Processes and Landforms*, *38*(3), 299–316. https://doi.org/10.1002/esp.3330

Anderson, R. S., Rajaram, H., & Anderson, S. P. (2019). Climate driven coevolution of weathering profiles and hillslope topography generates dramatic differences in critical zone architecture. *Hydrological Processes*, *33*(1), 4–19. https://doi.org/10.1002/hyp.13307

Anderson, S. P., Hinckley, E.-L., Kelly, P., & Langston, A. (2014). Variation in critical zone processes and architecture across slope aspects. *Procedia Earth and Planetary Science*, *10*, 28–33. https://doi.org/10.1016/j.proeps.2014.08.006

Anderson, S. P., Kelly, P. J., Hoffman, N., Barnhart, K., Befus, K., & Ouimet, W. (2021). Is this steady state? Weathering and critical zone architecture in Gordon Gulch, Colorado Front Range. *Hydrogeology, Chemical Weathering, and Soil Formation*, 231–252. https://doi.org/10.1002/9781119563952.ch13

Armesto, J. J., & Martinez, J. A. (1978). Relations between vegetation structure and slope aspect in the Mediterranean Region of Chile. *Journal of Ecology*, *66*(3), 881–889. https://doi.org/10.2307/2259301

Befus, K. M., Sheehan, A. F., Leopold, M., Anderson, S. P., & Anderson, R. S. (2011). Seismic constraints on critical zone architecture, Boulder Creek Watershed, Front Range, Colorado. *Vadose Zone Journal*, *10*(3), 915–927. https://doi.org/10.2136/vzj2010.0108

Berkland, J. O., Raymond, L. A., Kramer, J. C., Moores, E. M., & O'Day, M. (1972). What is Franciscan? *American Association of Petroleum Geologists Bulletin*, *56*, 2295–2302. https://doi.org/10.1306/819A421A-16C5-11D7-8645000102C1865D

Black, T. A., & Montgomery, D. R. (1991). Sediment transport by burrowing mammals, Marin County, California. *Earth Surface Processes and Landforms*, *16*(2), 163–172. https://doi.org/10.1002/esp.3290160207

Bolhar, R., & Ring, U. (2001). Deformation history of the Yolla Bolly terrane at Leech Lake Mountain, Eastern belt, Franciscan subduction complex, California Coast Ranges. *GSA Bulletin*, *113*(2), 181–195. https://doi.org/10.1130/0016-7606(2001)113<0181:DHOTYB>2.0.CO;2

Brantley, S. L., Lebedeva, M. I., Balashov, V. N., Singha, K., Sullivan, P. L., & Stinchcomb, G. (2017). Toward a conceptual model relating chemical reaction fronts to water flow paths in hills. *Geomorphology*, *277*, 100–117. https://doi.org/10.1016/j.geomorph.2016.09.027

Buss, H. L., Chapela Lara, M., Moore, O. W., Kurtz, A. C., Schulz, M. S., & White, A. F. (2017). Lithological influences on contemporary and long-term regolith weathering at the Luquillo Critical Zone Observatory. *Geochimica et Cosmochimica Acta*, *196*, 224–251. https://doi.org/10.1016/j.gca.2016.09.038

Byrne, R., Edlund, E., & Mensing, S. A. (1991). Holocene changes in the distribution and abundance of oaks in California. USDA Forest Service General Technical Report PSW-126 (pp. 182–188). Retrieved from http://treesearch.fs.fed.us/pubs/28418

Callahan, R. P., Riebe, C. S., Sklar, L. S., Pasquet, S., Ferrier, K. L., Hahm, W. J., et al. (2022). Forest vulnerability to drought controlled by bedrock composition. *Nature Geoscience*, *15*(9), 714–719. https://doi.org/10.1038/s41561-022-01012-2

Cannon, J. B., Peterson, C. J., O'Brien, J. J., & Brewer, J. S. (2017). A review and classification of interactions between forest disturbance from wind and fire. *Forest Ecology and Management*, *406*, 381–390. https://doi.org/10.1016/j.foreco.2017.07.035

Cassiani, G., Godio, A., Stocco, S., Villa, A., Deiana, R., Frattini, P., & Rossi, M. (2009). Monitoring the hydrologic behavior of a mountain slope via time-lapse electrical resistivity tomography. *Near Surface Geophysics*, *7*(5–6), 475–486. https://doi.org/10.3997/1873-0604.2009013

Chorover, J., Troch, P. A., Rasmussen, C., Brooks, P. D., Pelletier, J. D., Breshears, D. D., et al. (2011). How water, carbon, and energy drive critical zone evolution: The Jemez-Santa Catalina critical zone observatory. *Vadose Zone Journal*, *10*(3), 884–899. https://doi.org/10.2136/vzj2010.0132

Cole, K. (1983). Late Pleistocene vegetation of Kings Canyon, Sierra Nevada, California. *Quaternary Research*, *19*(1), 117–129. https://doi.org/10.1016/0033-5894(83)90031-5

Corlett, R. T., & Westcott, D. A. (2013). Will plant movements keep up with climate change? *Trends in Ecology & Evolution*, *28*(8), 482–488. https://doi.org/10.1016/j.tree.2013.04.003

Crawford, K. E. (1975). The geology of the Franciscan tectonic assemblage near Mount Hamilton, California (Ph.D. thesis), University of California, (p. 137).

Daniels, M. L., Anderson, R. S., & Whitlock, C. (2005). Vegetation and fire history since the Late Pleistocene from the Trinity Mountains, northwestern California, USA. *The Holocene*, *15*(7), 1062–1071. https://doi.org/10.1191/0959683605hl878ra

Desta, F., Colbert, J. J., Rentch, J. S., & Gottschalk, K. W. (2004). Aspect induced differences in vegetation, soil, and microclimatic characteristics of an Appalachian watershed. *Castanea*, *69*(2), 92–108. https://doi.org/10.2179/0008-7475(2004)069<0092:aidivs>2.0.co;2

Dibblee, T. W., Jr., & Minch, J. A. (2005). *Geologic map of the Diablo quad-rangle, contra costa and alameda counties*. Dibblee Geo-logical Foundation (Santa Barbara Museum of Natural History). Dibblee Foundation Map DF-162, scale 1:24,000.

Dixon, J., Heimsath, A., & Amundson, R. (2009). The critical role of climate and saprolite weathering in landscape evolution. *Earth Surface Processes and Landforms*, *34*, 155–161. https://doi.org/10.1002/esp

Doane, T. H., Edmonds, D., Yanites, B. J., & Lewis, Q. (2021). Topographic roughness on forested hillslopes: A theoretical approach for quantifying hillslope sediment flux from tree throw. *Geophysical Research Letters*, *48*(20), 1–10. https://doi.org/10.1029/2021GL094987

Donaldson, A. M. (2023). *Symmetry in hillslope steepness and saprolite thickness between hillslopes with opposing aspects*. HydroShare. Retrieved from http://www.hydroshare.org/resource/9a9897aa0bb14d20ab4189b98a8439f6

Ernst, W. G. (2011). Accretion of the Franciscan Complex attending Jurassic-Cretaceous geotectonic development of northern and central California. *Bulletin of the Geological Society of America*, *123*(9–10), 1667–1678. https://doi.org/10.1130/B30398.1

Fan, Y., Clark, M., Lawrence, D. M., Swenson, S., Band, L. E., Brantley, S. L., et al. (2019). Hillslope hydrology in global change research and Earth system modeling. *Water Resources Research*, *55*(2), 1737–1772. https://doi.org/10.1029/2018WR023903

Fan, Y., Grant, G., & Anderson, S. P. (2019). Water within, moving through, and shaping the Earth's surface: Introducing a special issue on water in the critical zone. *Hydrological Processes*, *33*(25), 3146–3151. https://doi.org/10.1002/hyp.13638

Ferdowsi, B., Gartner, J. D., Johnson, K. N., Kasprak, A., Miller, K. L., Nardin, W., et al. (2021). Earthcasting: Geomorphic forecasts for society. *Earth's Future*, *9*(11), 1–24. https://doi.org/10.1029/2021EF002088

Flinchum, B., Holbrook, W. S., Grana, D., Parsekian, A. D., Carr, B. J., Hayes, J. L., & Jiao, J. (2019). Estimating water holding capacity of the critical zone using near-surface geophysics. *Hydrological Processes*, *32*(22), 3308–3326. https://doi.org/10.1002/hyp.13260

Flinchum, B. A., Holbrook, W. S., & Carr, B. J. (2022). What do P-wave velocities tell us about the critical zone? *Frontiers in Water*, *3*, 1–15. https://doi.org/10.3389/frwa.2021.772185

Flinchum, B. A., Holbrook, W. S., Rempe, D., Moon, S., Riebe, C. S., Carr, B. J., et al. (2018). Critical zone structure under a granite ridge inferred from drilling and three-dimensional seismic refraction data. *Journal of Geophysical Research: Earth Surface*, *123*(6), 1317–1343. https://doi.org/10.1029/2017JF004280

Gabet, E. J., & Mudd, S. M. (2010). Bedrock erosion by root fracture and tree throw: A coupled biogeomorphic model to explore the humped soil production function and the persistence of hillslope soils. *Journal of Geophysical Research*, *115*(4), 1–14. https://doi.org/10.1029/2009JF001526

Gabet, E. J., Reichman, O. J., & Seabloom, E. W. (2003). The effects of bioturbation on soil processes and sediment transport. *Annual Review of Earth and Planetary Sciences*, *31*(1), 249–273. https://doi.org/10.1146/annurev.earth.31.100901.141314

García-Gamero, V., Peña, A., Laguna, A. M., Giráldez, J. V., & Vanwalleghem, T. (2021). Factors controlling the asymmetry of soil moisture and vegetation dynamics in a hilly Mediterranean catchment. *Journal of Hydrology*, *598*, 126207. https://doi.org/10.1016/j.jhydrol.2021.126207

Geldart, L. P., & Sheriff, R. E. (2004). *Problems in exploration seismology and their solutions*. Society of Exploration Geophysicists.

Götmark, F., & Kiffer, C. (2014). Regeneration of oaks (Quercus robur/Q. petraea) and three other tree species during long-term succession after catastrophic disturbance (windthrow). *Plant Ecology*, *215*(9), 1067–1080. https://doi.org/10.1007/s11258-014-0365-4

Granger, D. E., Kirchner, J. W., & Finkel, R. (1996). Spatially averaged long-term erosion rates measured from in situ-produced cosmogenic nuclides in alluvial sediment. *The Journal of Geology*, *104*(3), 249–257. https://doi.org/10.1086/629823

Gu, X., Mavko, G., Ma, L., Oakley, D., Accardo, N., Carr, B. J., et al. (2020). Seismic refraction tracks porosity generation and possible CO_2 production at depth under a headwater catchment. *Proceedings of the National Academy of Sciences of the United States of America*, *117*(32), 18991–18997. https://doi.org/10.1073/pnas.2003451117

Gutierrez-Jurado, H., Vivoni, E. R., Harrison, B. J., & Guan, H. (2006). Ecohydrology of root zone water fluxes and soil development in complex semiarid rangelands. *Hydrological Processes*, *20*(15), 2267–2274. https://doi.org/10.1002/hyp.6333

Hagedorn, F., Gavazov, K., & Alexander, J. M. (2019). Above- and belowground linkages shape responses of mountain vegetation to climate change. *Science*, *1123*, 1119–1123. https://doi.org/10.1126/science.aax4737

Hahm, W. J., Dralle, D. N., Sanders, M., Bryk, A. B., Fauria, K. E., Huang, M. H., et al. (2022). Bedrock vadose zone storage dynamics under extreme drought: Consequences for plant water availability, recharge, and runoff. *Water Resources Research*, *58*(4), 1–23. https://doi.org/10.1029/2021WR031781

Hahm, W. J., Rempe, D. M., Dralle, D. N., Dawson, T. E., & Dietrich, W. E. (2020). Oak transpiration drawn from the weathered bedrock vadose zone in the summer dry season. *Water Resources Research*, *56*(11), 1–24. https://doi.org/10.1029/2020WR027419

Hahm, W. J., Rempe, D. M., Dralle, D. N., Dawson, T. E., Lovill, S. M., Bryk, A. B., et al. (2019). Lithologically controlled subsurface critical zone thickness and water storage capacity determine regional plant community composition. *Water Resources Research*, *55*(4), 3028–3055. https://doi.org/10.1029/2018WR023760

Hall, K., & Lamont, N. (2003). Zoogeomorphology in the Alpine: Some observations on abiotic–biotic interactions. *Geomorphology*, *55*(1–4), 219–234. https://doi.org/10.1016/S0169-555X(03)00141-7

Hasenmueller, E. A., Gu, X., Weitzman, J. N., Adams, T. S., Stinchcomb, G. E., Eissenstat, D. M., et al. (2017). Weathering of rock to regolith: The activity of deep roots in bedrock fractures. *Geoderma*, *300*, 11–31. https://doi.org/10.1016/j.geoderma.2017.03.020

Hayes, J. L., Riebe, C. S., HolbrookFlinchum, S. W. B. A., & Hartsough, P. C. (2019). Porosity production in weathered rock: Where volumetric strain dominates over chemical mass loss. *Science Advances*, *5*(9), 1–12. https://doi.org/10.1126/sciadv.aao0834

Heimsath, A. M., Dietrich, W. E., Nishiizumi, K., & Finkel, R. C. (1999). Cosmogenic nuclides, topography, and the spatial variation of soil depth. *Geomorphology*, *27*(1–2), 151–172. https://doi.org/10.1016/S0169-555X(98)00095-6

Heusser, L. (1998). Direct correlation of millennial-scale changes in western North American vegetation and climate with changes in the California current system over the past ~60 Kyr. *Paleoceanography*, *13*(3), 252–262. https://doi.org/10.1029/98PA00670

Huang, M. H., Hudson-Rasmussen, B., Burdick, S., Lekic, V., Nelson, M. D., Fauria, K. E., & Schmerr, N. (2021). Bayesian seismic refraction inversion for critical zone science and near-surface applications. *Geochemistry, Geophysics, Geosystems*, *22*(5), 1–20. https://doi.org/10.1029/2020GC009172

Hudson-Rasmussen, B., Huang, M.-H., Hahm, W. J., Rempe, D., Dralle, D. N., & Nelson, M. D. (2023). Mapping variations in bedrock weathering with slope aspect under a sedimentary ridge–valley system using near–surface geophysics and drilling. *ESS Open Archive*. https://doi.org/10.22541/essoar.168435460.02903987/v1

Hughes, M. W., Almond, P. C., & Roering, J. J. (2009). Increased sediment transport via bioturbation at the last glacial-interglacial transition. *Geology*, *37*(10), 919–922. https://doi.org/10.1130/G30159A.1

Inbar, A., Nyman, P., Rengers, F. K., Lane, P. N. J., & Sheridan, G. J. (2018). Climate dictates magnitude of asymmetry in soil depth and hillslope gradient. *Geophysical Research Letters*, *45*(13), 6514–6522. https://doi.org/10.1029/2018GL077629

Istanbulluoglu, E., Yetemen, O., Vivoni, E. R., Gutiérrez-Jurado, H. A., & Bras, R. L. (2008). Eco-geomorphic implications of hillslope aspect: Inferences from analysis of landscape morphology in central New Mexico. *Geophysical Research Letters*, *35*(14), 1–6. https://doi.org/10.1029/2008GL034477

Ivory, S. J., Mcglue, M. M., Ellis, G. S., Lézine, A.-M., Cohen, A. S., & Vincens, A. (2014). Vegetation controls on weathering intensity during the last deglacial transition in southeast Africa. *PLoS One*, *9*(11), 112855. https://doi.org/10.1371/journal.pone.0112855

Jackson, R. B., Schenk, H. J., Jobbágy, E. G., Canadell, J., Colello, G. D., Dickinson, R. E., et al. (2000). Belowground consequences of vegetation change and their treatment in models. *Ecological Applications*, *10*(2), 470–483. https://doi.org/10.1890/1051-0761(2000)010[0470:BCOVCA]2.0.CO;2

Kanso, T., Gromaire, M. C., Ramier, D., Dubois, P., & Chebbo, G. (2020). An investigation of the accuracy of EC5 and 5TE capacitance sensors for soil moisture monitoring in urban soils-laboratory and field calibration. *Sensors*, *20*(22), 6510. https://doi.org/10.3390/s20226510

Kulongoski, J. T., Hilton, D. R., Izbicki, J. A., & Belitz, K. (2009). Evidence for prolonged El Nino-like conditions in the Pacific during the Late Pleistocene: A 43 ka noble gas record from California groundwaters. *Quaternary Science Reviews*, *28*(23–24), 2465–2473. https://doi.org/10.1016/j.quascirev.2009.05.008

Kumari, N., Saco, P. M., Rodriguez, J. F., Johnstone, S. A., Srivastava, A., Chun, K. P., & Yetemen, O. (2020). The grass is not always greener on the other side: Seasonal reversal of vegetation greenness in aspect-driven semiarid ecosystems. *Geophysical Research Letters*, *47*(15), 1–12. https://doi.org/10.1029/2020GL088918

Langston, A. L., Tucker, G. E., Anderson, R. S., & Anderson, S. P. (2015). Evidence for climatic and hillslope-aspect controls on vadose zone hydrology and implications for saprolite weathering. *Earth Surface Processes and Landforms*, *40*(9), 1254–1269. https://doi.org/10.1002/esp.3718

Lebedeva, M. I., & Brantley, S. L. (2013). Exploring geochemical controls on weathering and erosion of convex hillslopes: Beyond the empirical regolith production function. *Earth Surface Processes and Landforms*, *38*(15), 1793–1807. https://doi.org/10.1002/esp.3424

Lebedeva, M. I., & Brantley, S. L. (2018). A clarification and extension of our model of regolith formation on hillslopes. *Earth Surface Processes and Landforms*, *43*(13), 2715–2723. https://doi.org/10.1002/esp.4426

Lebedeva, M. I., & Brantley, S. L. (2020). Exploring an 'ideal hill': How lithology and transport mechanisms affect the possibility of a steady state during weathering and erosion. *Earth Surface Processes and Landforms*, *45*(3), 652–665. https://doi.org/10.1002/esp.4762
Leone, J. D., Holbrook, W. S., Riebe, C. S., Chorover, J., Ferré, T. P. A., Carr, B. J., & Callahan, R. P. (2020). Strong slope-aspect control of regolith thickness by bedrock foliation. *Earth Surface Processes and Landforms*, *45*(12), 2998–3010. https://doi.org/10.1002/esp.4947
Lucas, Y. (2001). The role of plants in controlling rates and products of weathering: Importance of biological pumping. *Annual Review of Earth and Planetary Sciences*, *29*(1), 135–163. https://doi.org/10.1146/annurev.earth.29.1.135
Ma, L., Oakley, D., Nyblade, A., Moon, S., Accardo, N., Wang, W., et al. (2021). Seismic imaging of a shale landscape under compression shows limited influence of topography-induced fracturing. *Geophysical Research Letters*, *48*(17), e2021GL093372. https://doi.org/10.1029/2021GL093372
Marshall, J. A., Roering, J. J., Rempel, A. W., Shafer, S. L., & Bartlein, P. J. (2021). Extensive frost weathering across unglaciated North America during the last glacial maximum. *Geophysical Research Letters*, *48*(5), e2020GL090305. https://doi.org/10.1029/2020GL090305
Maxwell, A. E., & Shobe, C. M. (2022). Land-surface parameters for spatial predictive mapping and modeling. *Earth-Science Reviews*, *226*, 103944. https://doi.org/10.1016/j.earscirev.2022.103944
McGuire, L. A., Pelletier, J. D., & Roering, J. J. (2014). Development of topographic asymmetry: Insights from dated cinder cones in the western United States. *Journal of Geophysical Research F: Earth Surface*, *119*(8), 1725–1750. https://doi.org/10.1002/2014JF003081
McKnight, P., & Najab, J. (2010). Mann-Whitney U test. *Dictionary of Statistics & Methodology*. https://doi.org/10.4135/9781412983907.n1115
Mensing, S. (2005). The history of oak woodlands in California, part I: The paleoecologic record.
Metropolis, N., Rosenbluth, A. W., Rosenbluth, M. N., Teller, A. H., & Teller, E. (1953). Equation of state calculations by fast computing machines. *The Journal of Chemical Physics*, *21*(6), 1087–1092. https://doi.org/10.1063/1.1699114
Montgomery, D. R. (1993). Compressional uplift in the central California Coast ranges. *Geology*, *21*(6), 543–546. https://doi.org/10.1130/0091-7613(1993)021<0543:CUITCC>2.3.CO;2
Moon, S., Perron, J. T., Martel, S. J., Holbrook, W. S., & St. Clair, J. (2017). A model of three-dimensional topographic stresses with implications for bedrock fractures, surface processes, and landscape evolution. *Journal of Geophysical Research: Earth Surface*, *122*(4), 823–846. https://doi.org/10.1002/2016JF00415
Nielson, T., Bradford, J., Holbrook, W. S., & Seyfried, M. (2021). The effect of aspect and elevation on critical zone architecture in the Reynolds Creek critical zone observatory: A seismic refraction study. *Frontiers in Wate*, *1*, 670524. https://doi.org/10.3389/frwa.2021.670524
Page, B. M. (1999). Geology of the lick observatory quadrangle, California. *International Geology Review*, *41*(4), 355–367. https://doi.org/10.1080/00206819909465146
Pawlik, Ł., Phillips, J. D., & Šamonil, P. (2016). Roots, rock, and regolith: Biomechanical and biochemical weathering by trees and its impact on hillslopes-A critical literature review. *Earth-Science Reviews*, *159*, 142–159. https://doi.org/10.1016/j.earscirev.2016.06.002
Pedrazas, M. A., Hahm, W. J., Huang, M.-H., Dralle, D., Nelson, M. D., Breunig, R. E., et al. (2021). The relationship between topography, bedrock weathering, and water storage across a sequence of ridges and valleys. *Journal of Geophysical Research: Earth Surface*, *126*(4), e2020JF005848. https://doi.org/10.1029/2020JF005848
Pelletier, J. D., Barron-Gafford, G. A., Gutiérrez-Jurado, H., Hinckley, E.-L. S., Istanbulluoglu, E., McGuire, L. A., et al. (2017). Which way do you lean? Using slope aspect variations to understand critical zone processes and feedbacks. *Earth Surface Processes and Landforms*, *43*(5), 1133–1154. https://doi.org/10.1002/esp.4306
Perron, J. T. (2017). Climate and the pace of erosional landscape evolution. *Annual Review of Earth and Planetary Sciences*, *45*, 1–71. https://doi.org/10.1146/annurev-earth-060614-105405
Poulos, M. J., Pierce, J. L., Flores, A. N., & Benner, S. G. (2012). Hillslope asymmetry maps reveal widespread, multi-scale organization. *Geophysical Research Letters*, *39*(6), 6406. https://doi.org/10.1029/2012GL051283
Raymond, L. A. (2014). Designating tectonostratigraphic terranes versus mapping rock units in subduction complexes: Perspectives from the Franciscan Complex of California, USA. *International Geology Review*, *57*(5–8), 801–823. https://doi.org/10.1080/00206814.2014.911124
Raymond, L. A. (2018). What is Franciscan?: Revisited. *International Geology Review*, *60*(16), 1968–2030. https://doi.org/10.1080/00206814.2017.1396933
Regmi, N. R., McDonald, E. V., & Rasmussen, C. (2019). Hillslope response under variable microclimate. *Earth Surface Processes and Landforms*, *44*(13), 2615–2627. https://doi.org/10.1002/esp.4686
Rempe, D. M., & Dietrich, W. E. (2014). A bottom-up control on fresh-bedrock topography under landscapes. *Proceedings of the National Academy of Sciences of the United States of America*, *111*(18), 6576–6581. https://doi.org/10.1073/pnas.1404763111
Riebe, C. S., Callahan, R. P., Granke, S. B. M., Carr, B. J., Hayes, J. L., Schell, M. S., & Sklar, L. S. (2021). Anisovolumetric weathering in granitic saprolite controlled by climate and erosion rate. *Geology*, *49*(5), 551–555. https://doi.org/10.1130/G48191.1551-555
Riebe, C. S., Kirchner, J. W., Granger, D. E., & Finkel, R. C. (2001). Strong tectonic and weak climatic control of long-term chemical weathering rates. *Geology*, *29*(6), 511–514. https://doi.org/10.1130/0091-7613(2001)029
Roering, J. J., Almond, P., McKean, J., & Tonkin, P. (2002). Soil transport driven by biological processes over millennial timescales. *Geology*, *30*(12), 1115–1118. https://doi.org/10.1130/0091-7613(2002)030<1115:STDBBP>2.0.CO;2
Šamonil, P., Egli, M., Steinert, T., Norton, K., Abiven, S., Daněk, P., et al. (2020). Soil denudation rates in an old-growth mountain temperate forest driven by tree uprooting dynamics, Central Europe. *Land Degradation & Development*, *31*(2), 222–239. https://doi.org/10.1002/ldr.3443
Sharp, R. P. (1982). Landscape evolution (A review). *Proceedings of the National Academy of Sciences of the United States of America*, *79*(14), 4477–4486. https://doi.org/10.1073/pnas.79.14.4477
Smith, T., & Bookhagen, B. (2020). Climatic and biotic controls on topographic asymmetry at the global scale. https://doi.org/10.1029/2020JF005692
Sólyom, P. B., & Tucker, G. (2004). Effect of limited storm duration on landscape evolution, drainage basin geometry, and hydrograph shapes. *Journal of Geophysical Research*, *109*(F3), 1–13. https://doi.org/10.1029/2003jf000032
St. Clair, J., Moon, S., Holbrook, W. S., Perron, J. T., Riebe, C. S., Martel, S. J., et al. (2015). Geophysical imaging reveals topographic stress control of bedrock weathering. *Science*, *350*(6260), 534–538. https://doi.org/10.1126/science.aab2210
Szwagrzyk, J., Gazda, A., Dobrowolska, D., Chećko, E., Zaremba, J., & Tomski, A. (2018). Natural regeneration following wind disturbance increases the diversity of managed lowland forests in NE Poland. *Journal of Vegetation Science*, *29*(5), 898–906. https://doi.org/10.1111/jvs.12672
Übernickel, K., Pizarro-Araya, J., Bhagavathula, S., Paulino, L., & Ehlers, T. A. (2021). Reviews and syntheses: Composition and characteristics of burrowing animals along a climate and ecological gradient, Chile. *Biogeosciences*, *18*(20), 5573–5594. https://doi.org/10.5194/bg-18-5573-2021
U.S. Geological Survey. (2020). 3D elevation program. CA LiDar. Distributed by OpenTopography Retrieved from https://portal.opentopography.org/usgsDataset?dsid=CA_SantaClaraCounty_2020

Wang, W., Chen, P., Dueker, K., Zhang, Y., Lee, E.-J., Mu, D., et al. (2021). Coevolution of weathering front and water table. *Geophysical Research Letters*, *48*(20), e2021GL092916. https://doi.org/10.1029/2021GL092916

Wentworth, C. M., Blake, M. C., Mclaughlin, R. J., & Graymer, R. W. (1999). Preliminary geologic description of the San Jose 30 X 60 minute quadrangle, California. *Open-File Report*, *98–795*, 1–52.

West, N., Kirby, E., Nyblade, A. A., & Brantley, S. L. (2019). Climate preconditions the Critical Zone: Elucidating the role of subsurface fractures in the evolution of asymmetric topography. *Earth and Planetary Science Letters*, *513*, 197–205. https://doi.org/10.1016/j.epsl.2019.01.039

Wiekenkamp, I., Huisman, J. A., Bogena, H. R., Lin, H. S., & Vereecken, H. (2016). Spatial and temporal occurrence of preferential flow in a forested headwater catchment. *Journal of Hydrology*, *534*, 139–149. https://doi.org/10.1016/j.jhydrol.2015.12.050

Yazici, B., & Yolacan, S. (2007). A comparison of various tests of normality. *Journal of Statistical Computation and Simulation*, *77*(2), 175–183. https://doi.org/10.1080/10629360600678310

Yetemen, O., Istanbulluoglu, E., Homero Flores-Cervantes, J., Vivoni, E., & Bras, R. (2015). Ecohydrologic role of solar radiation on landscape evolution, 1127–1157. https://doi.org/10.1002/2014WR016169

Zapata-Rios, X., Brooks, P. D., Troch, P. A., McIntosh, J., & Guo, Q. (2016). Influence of terrain aspect on water partitioning, vegetation structure and vegetation greening in high-elevation catchments in northern New Mexico. *Ecohydrology*, *9*(5), 782–795. https://doi.org/10.1002/eco.1674

Zhou, X., Istanbulluoglu, E., & Vivoni, E. R. (2013). Modeling the ecohydrological role of aspect-controlled radiation on tree-grass-shrub coexistence in a semiarid climate. *Water Resources Research*, *49*(5), 2872–2895. https://doi.org/10.1002/wrcr.20259